Chemical Engineering Journal 167 (2011) 603–609

Contents lists available at ScienceDirect

Chemical Engineering Journal

journal homepage: www.elsevier.com/locate/cej

Computational fluid dynamics simulation of ethanol steam reforming in catalytic wall microchannels

I. Uriz [a], G. Arzamendi [a], E. López [b,c], J. Llorca [b], L.M. Gandía [a,*]

[a] Departamento de Química Aplicada, Edificio de los Acebos, Universidad Pública de Navarra, Campus de Arrosadía s/n, E-31006 Pamplona, Spain
[b] Institut de Tècniques Energètiques, Universitat Politècnica de Catalunya, Diagonal 647, ed. ETSEIB, 08028 Barcelona, Spain
[c] Planta Piloto de Ingeniería Química (CONICET-UNS), Camino de la Carridanga km7, 8000 Bahía Blanca, Argentina

ARTICLE INFO

Article history:
Received 30 March 2010
Received in revised form 22 July 2010
Accepted 24 July 2010

Keywords:
Computational fluid dynamics (CFD)
Ethanol steam reforming
Hydrogen
Microchannel reactor
Microreactor

ABSTRACT

A three-dimensional computational fluid dynamics (CFD) simulation study of the ethanol steam reforming (ESR) in microreactors with square channels has been carried out. A phenomenological kinetic model describing the ESR on a Co_3O_4–ZnO catalyst has been established and implemented in the CFD codes. This model includes the ethanol dehydrogenation to acetaldehyde, ethanol decomposition to CO and CH_4, acetaldehyde steam reforming to H_2 and CO_2 and water–gas shift as the reactions describing the catalyst behavior. The very different thermal effects and apparent activation energies of these reactions allow interpreting the influence of the main operating parameters on the microreactors performance. The high activation energy and relatively low energy demand of the ethanol decomposition limit the production of hydrogen at high temperatures and space velocities (up to 70,000 h^{-1}) at yields of the order of 70%, that is, 4.2 mol of H_2 per mol of ethanol fed into the reactor. Another issue is the presence of significant CO contents in the reformate stream. This can be partially solved by increasing the catalyst loading which leads to a lower temperature and then an improved selectivity to ethanol dehydrogenation and acetaldehyde reforming. The microchannel characteristic size in the 0.10–0.70 mm range has a strong influence on the microreactor performance that is mainly governed by the surface area-to-volume ratio. For the smallest sizes considered in this study (0.10 and 0.35 mm) it has been found that the flow of the gases is nearly isothermal.

1. Introduction

Hydrogen can be produced from a variety of feedstocks. Among them, ethanol is very promising due to its high hydrogen content, availability, low toxicity and easy storage and distribution [1–4]. Most importantly, ethanol can be produced from biomass-derived materials such as starch and lignocelluloses coming from agricultural wastes and forestry residues thus leading to the possibility of obtaining renewable hydrogen [5,6]. Reforming bioethanol with steam is particularly attractive because bioethanol, which is a dilute aqueous solution containing about 12 wt.% ethanol, could be directly used, thus eliminating the costly separation processes required to obtain pure ethanol [2,4].

Ethanol steam reforming (ESR) can be ideally represented by the following reaction:

$$C_2H_5OH(g) + 3H_2O(g) \rightarrow 2CO_2 + 6H_2 \quad (\Delta H^\circ_{298\,K} = 174\,kJ/mol) \tag{1}$$

However, undesired reactions can take place resulting in the formation of other products such as acetaldehyde, ethylene, acetone, CO, CH_4 and coke. In order to obtain high hydrogen yields and minimize the formation of side products, high temperatures (400–700 °C), atmospheric pressure, high water-to-ethanol molar ratios in the feed (6 or above) and suitable catalysts are required [1,2]. It should be noted that at sufficiently high temperatures the ESR is not thermodynamically limited being the equilibrium ethanol conversion always 100%. On the other hand, obtaining high hydrogen yields and very low CO contents during ESR is difficult because at the high temperatures required the reverse water–gas shift (r-WGS) reaction is thermodynamically favoured, although its influence can be limited to some extent using high water-to-ethanol ratios [7]:

$$H_2 + CO_2 \leftrightarrow CO + H_2O \quad (\Delta H^\circ_{298\,K} = 41\,kJ/mol) \tag{2}$$

There is a growing interest in microstructured reactors for fuel conversion applications, particularly for hydrogen production, because these devices can cover the needs of portable, transportation and small-scale decentralized stationary systems, much of them based on fuel cells [8–10]. These uses require compact, light,

* Corresponding author. Tel.: +34 948 169605; fax: +34 948 169606.
E-mail address: lgandia@unavarra.es (L.M. Gandía).

1385-8947/$ – see front matter © 2010 Elsevier B.V. All rights reserved.
doi:10.1016/j.cej.2010.07.070

efficient, highly dynamic and integrated fuel processors. Moreover, reforming reactions are strongly endothermic (see Eq. (1)), therefore thermal integration through the coupling of reforming with the combustion of part of the fuel or the fuel cell anode off-gas needs very high heat transfer rates [9–11]. The high surface area-to-volume ratio and heat transfer coefficients characteristic of microreactors make these devices suitable for fast highly exothermic or endothermic reactions because they allow nearly isothermal operation avoiding hot-spots formation [12].

Compared with the case of methanol [13,14], the number of ethanol processors reported in the literature is scarce. For example, a combined ethanol steam reformer–anode off-gas afterburner with a power output of 250 W has been constructed at IMM (Institut für Mikrotechnik Mainz, Germany). Design was based on plate heat exchanger technology using Co/ZnO as reforming catalyst [14]. Benito et al. [15] built and operated a bioethanol processor based on steam reforming designed for a power output of 1 kW. A multi-fuel processor (including ethanol) was constructed in the framework of a Renault/Nuvera Fuel Cells joint program. Operation at very high powers of up to 180 kW_{th} has been reported [16]. Autothermal reforming of ethanol has been implemented in a portable processor with a 250 W_{el} fuel cell system [17]. Other studies conducted in microchannel reactors at substantially lower levels of hydrogen production have revealed a good performance of Rh and Ir catalysts supported on CeO_2 for ESR [18–20]. As concerns non-noble metals-based catalysts, results by Llorca and coworkers have shown the potential of the Co/ZnO and Co_3O_4–ZnO systems for conducting the ethanol steam reforming at temperatures as low as 450 °C with good selectivity and yield; methods for efficiently washcoat the walls of microchannels and micromonoliths with these catalysts were also developed [21–24]. Several simulation studies investigating energy integration strategies, performance and controllability of ethanol processors have been also reported [25–28].

To the best of our knowledge, this work is the first computational fluid dynamics (CFD) simulation study on ESR in microchannel reactors. The kinetic equations of the relevant chemical reactions over a Co_3O_4–ZnO catalyst have been established and implemented in CFD codes with the aim of investigating the effects of the characteristic dimension, catalyst loading, space velocity and heat supply on the microreactor performance.

2. Kinetic model

In order to investigate the reaction kinetics, ethanol steam reforming reactions were performed in a silicon micromonolithic reactor described in detail in a previous work [29]. The silicon-based microreformer consisted in three in-series silicon wafers with ca. 8×10^6 circular channels of ca. 3 μm in diameter. The channels walls were functionalized with a Co_3O_4–ZnO catalyst layer following the method described in [23,24,29]. The wafers were mounted into a stainless steel casing with liquid evaporators and electrical heating. Kinetic experiments were carried out at atmospheric pressure, temperatures in the 400–500 °C range and feed streams containing undiluted mixtures with H_2O/ethanol molar ratios of 3, 6 and 13. Total liquid feed flow rates were in the 0.18–5.4 mL/h range resulting in contact times between 30 and 900 ms and ethanol conversions between 20 and 100%. On-line analysis of the product stream was performed on a micro-GC (Agilent 3000A) equipped with MS 5 Å, Plot U and Stabilwax columns. Catalytic activity was stable during the experiments and H_2, CO, CO_2, CH_4 and acetaldehyde were the main reaction products; only negligible amount of ethane, ethylene and acetone were formed.

As already reported in the literature [22,30,31], the following reaction scheme given by Eqs. (3)–(6) applies to describe the ESR over cobalt-based catalysts:

$$C_2H_5OH \xrightarrow{k_3} CH_3CHO + H_2 \quad (\Delta H^\circ_{723\,K} = 71.0\,kJ/mol) \tag{3}$$

$$C_2H_5OH \xrightarrow{k_4} CO + CH_4 + H_2 \quad (\Delta H^\circ_{723\,K} = 52.9\,kJ/mol) \tag{4}$$

$$CO + H_2O \overset{k_5, K_{WGS}}{\longleftrightarrow} CO_2 + H_2 \quad (\Delta H^\circ_{723\,K} = -34.5\,kJ/mol) \tag{5}$$

$$CH_3CHO + 3H_2O \xrightarrow{k_6} 2CO_2 + 5H_2 \quad (\Delta H^\circ_{723\,K} = 127.4\,kJ/mol) \tag{6}$$

It has been demonstrated that the simultaneous presence of metallic cobalt and cobalt oxide is required for the progress of the reaction. In fact, ethanol dehydrogenates into hydrogen and acetaldehyde over cobalt oxide (Eq. (3)), which is further reformed with water to carbon dioxide over metallic cobalt (Eq. (6)). In addition, cobalt catalysts are active for the water–gas shift (WGS) reaction (Eq. (5)) under typical operating conditions. An undesired source of carbon monoxide and methane is the ethanol decomposition, as indicated by Eq. (4).

A phenomenological kinetic model with power-law rate expressions has been developed including the following set of equations:

$$r_3 = k_3 \cdot P_{C_2H_5OH} \tag{7}$$

$$r_4 = k_4 \cdot P_{C_2H_5OH} \tag{8}$$

$$r_5 = k_5 \cdot \left(P_{CO} \cdot P_{H_2O} - \frac{P_{CO_2} \cdot P_{H_2}}{K_{WGS}} \right) \tag{9}$$

$$r_6 = k_6 \cdot P_{CH_3CHO} \cdot P^3_{H_2O} \tag{10}$$

$$k_i = k^{ref} \cdot \exp\left(\frac{-E_i}{R} \left(\frac{1}{T} - \frac{1}{T^{ref}} \right) \right); \quad T^{ref} = 773\,K \tag{11}$$

$$K_{WGS} = \exp\left(\frac{4577.8}{T} - 4.33 \right) \tag{12}$$

where P_i (bar) are the corresponding partial pressures, k_i the kinetic constants, k_i^{ref} the kinetic constants at the reference temperature of 500 °C, E_i the apparent activation energies, K_{WGS} the equilibrium constant of the WGS reaction and R the universal gas constant. A steady-state, one-dimensional, isothermal pseudo-homogeneous mathematical model of the silicon microreactor was adopted. Estimation of the kinetic parameters was conducted using a nonlinear multiparametric regression algorithm [32]. A satisfactory fit of the model to the experimental data was achieved with the values of the parameters included in Table 1.

Table 1
Estimated kinetic parameters of the rate equations indicated.[a]

Equation (i)	k_i^{ref}	E_i (kJ/mol)
(3)	2.1×10^4 [mol/(m^3 min bar)]	70
(4)	2.0×10^3 [(mol/(m^3 min bar)]	130
(5)	1.9×10^4 [mol/(m^3 min bar^2)]	70
(6)	2.0×10^5 [mol/(m^3 min bar^4)]	98

[a] Kinetic constants are given at the reference temperature of 500 °C.

3. Microreactor model and simulation conditions

Three-dimensional simulations have been carried out with the software package ANSYS CFX that has provided satisfactory results in previous studies [33–36]. Simulations were conducted on a Dell Precision PWS690 workstation running MS Windows XP® × 64 with available RAM of 16.0 GB.

A physical model (Fig. 1A) consisting of square parallel microchannels of 20 mm of length and 0.10, 0.35 and 0.70 mm of side (d) was developed to investigate the influence of the channels size and the operating variables on the microreactor performance. This model has been used previously to study the steam reforming

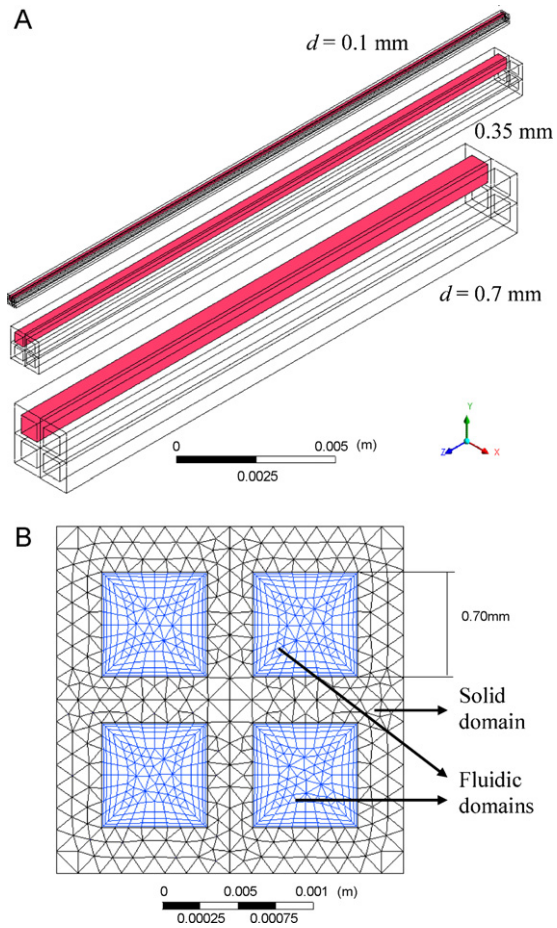

Fig. 1. (A) Geometric models of the microreactors with square channels of 0.10, 0.35 and 0.70 mm of side. (B) Unstructured mesh applied to the solid and fluidic domains.

of methane and methanol and is described in more detail elsewhere [34,35]. The model has two types of physical domains (Fig. 1B), one of them is fluidic and the other is the solid block (silicon). The physical spaces of these domains were divided into a mesh with control volumes where the governing equations are solved iteratively until the established criteria of convergence are fulfilled. The total number of elements (prisms and hexahedrons) amounted up to 152,800. In order to resolve the boundary layers accurately a mixed unstructured grid approach was applied in the fluidic domain near the solid walls.

When working in micro fluidics it is very important to check the validity of the continuum model and evaluate possible rarefied gas flow effects [37]. To this end, the Knudsen number (Kn) has been evaluated for the most unfavourable situation, that is, for the smallest channel (d = 0.10 mm), resulting in values of Kn between 8×10^{-4} and 1×10^{-3}, which are sufficiently low as to assure the validity of the continuum model and the Navier–Stokes equations for the systems considered in this work [38]. On the other hand, the Reynolds numbers are between 0.5 and 51, so the flow regime of the gases is clearly laminar.

Catalytic reactions were modeled considering the microchannels walls as sources of products and sinks of reactants [34,35]. The kinetic model formed by Eqs. (7)–(12) and the parameters included in Table 1 were implemented in the CFD code. It has been assumed that a thin layer of a Co_3O_4–ZnO catalyst [22–24] was uniformly deposited onto the walls of the microreactors at loadings of 1, 2 and 4 mg/cm^2. The feedstream was composed by steam and ethanol at a molar ratio of 6:1 and the inlet temperature was set at 450 °C. Gas hourly space velocities (GHSV) in the range between 5250 and 70,000 h^{-1} (STP) have been considered. To give an idea, this is equivalent to feed the microchannel with 0.70 mm of side with 0.84–11.12 mL/min (STP) of the reaction mixture. Simulations have been conducted under stationary conditions. The external walls of the block were considered adiabatic and homogeneous heat generation inside the solid was adopted to emulate the presence of heating cartridges. Thermophysical properties of silicon at 527 °C were used for the solid material (density = 2330 kg/m^3; specific heat = 913 J/(kg °C); thermal conductivity = 42.2 W/(m °C)) [39].

4. Results and discussion

4.1. Effect of the space velocity and heat supply

A series of CFD simulations was conducted with a reforming catalyst loading of 1 mg/cm^2 and heat supplies between 250 and 375 kJ/mol of ethanol fed into the reactor. The evolution of the mean ethanol conversion and reforming temperature at the microchannels (d = 0.70 mm) outlet with respect to the space velocity are shown in Fig. 2A. It can be seen that both the ethanol conversion and outlet temperature are very sensitive to the heat supply and increase with this parameter. As indicated in Eq. (1), the ESR requires 174 kJ/mol, which is an amount significantly lower than the heat supplies considered in these simulations. Obviously this is because the reforming reaction is feasible only at sufficiently high temperatures so more energy is necessary to heat up the feed stream entering the microchannels at 450 °C. Up to 375 kJ/mol of ethanol fed into the microreactor are required in this case to obtain ethanol conversions about 95%. However, the ethanol conversion is only 60–70% if the heat supply is decreased to 250 kJ/mol.

Hydrogen is produced by all the reactions involved in the ESR (see Eqs. (3)–(6)), so the hydrogen yield (Fig. 2B) follows a trend similar to that of the ethanol conversion. In the most favourable case (375 kJ/mol), the hydrogen yield varies from about 75% at GHSV of 5250 h^{-1} to 60% at 70,000 h^{-1}, that is, from 4.5 to 3.6 mol of H_2 per mol of ethanol fed into the reactor.

As the space velocity increases the outlet temperature significantly increases for a given heating supply. This indicates that a lesser fraction of the energy provided is being consumed as reaction heat. However, the ethanol conversion decreases with the GHSV only very slightly (Fig. 2A). The selectivities to carbon-containing products for the simulations performed with a heating supply of 375 kJ/mol are shown in Fig. 2C. It can be seen that the selectivities to both CO_2 and acetaldehyde decrease in a parallel way with the space velocity whereas that to methane and CO increase. This means that the ethanol decomposition (Eq. (4)) is being favoured. This is the reaction with less energy demand (52.9 kJ/mol) and thus more heat is available that increases the temperature. Moreover, ethanol decomposition exhibits the highest apparent activation energy (see Table 1) and therefore is further favoured by the temperature increase. In contrast, less ethanol is dehydrogenated to acetaldehyde (Eq. (3)), which gives up to 5 mol of hydrogen upon steam reforming (Eq. (6)). This results in a clear decrease of the hydrogen yield with increasing space velocity values, as it is apparent in Fig. 2B. This is a negative feature of the ESR reaction system that limits the operation at high space velocities because the hydrogen yield decreases and the CO content of the reformate increases. CO is a well-known poison of the electrocatalysts used in the low-temperature polymer electrolyte membrane fuel cells (PEMFC). However, the presence of acetaldehyde is not positive either because it decomposes on the PEMFC electrocatalysts generating more CO [40].

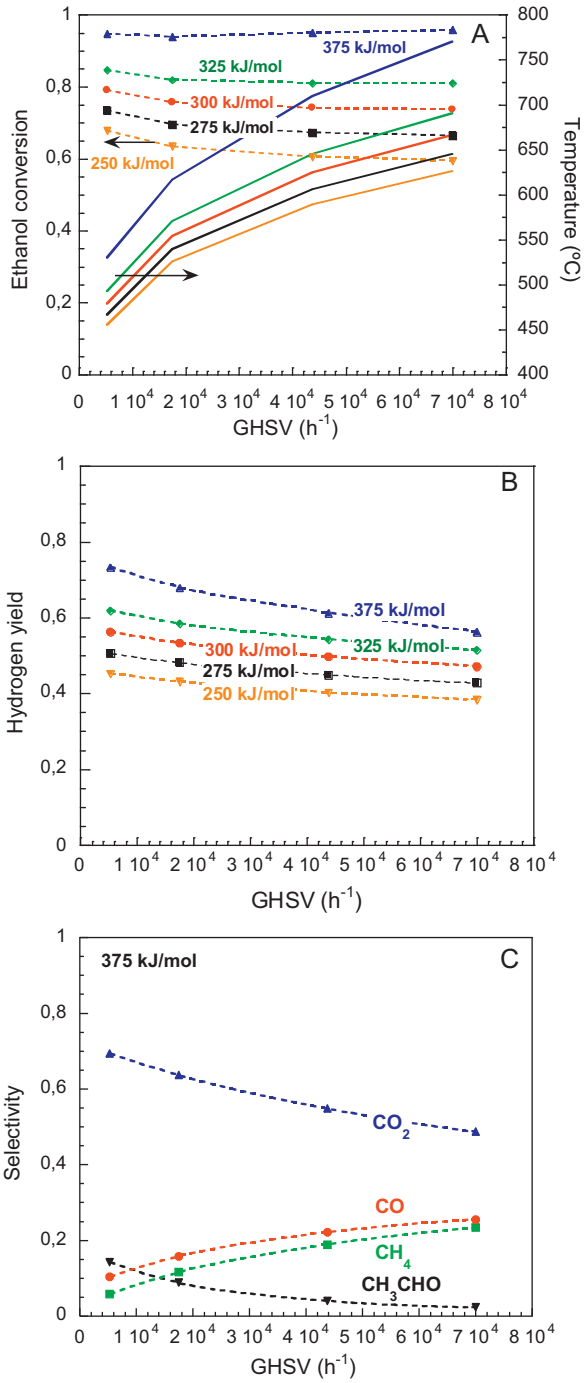

Fig. 2. (A) Ethanol conversion and mean reforming temperatures (solid lines). (B) Hydrogen yields. (C) Selectivities to CO_2, CO, CH_4 and acetaldehyde. Simulations were performed for microchannels with 0.70 mm of side, catalyst loading of 1 mg/cm^2 and heating supplies (A and B) of 250 (orange), 275 (black), 300 (red), 325 (green) and 375 kJ/mol (blue). (For interpretation of the references to color in this figure legend, the reader is referred to the web version of the article.)

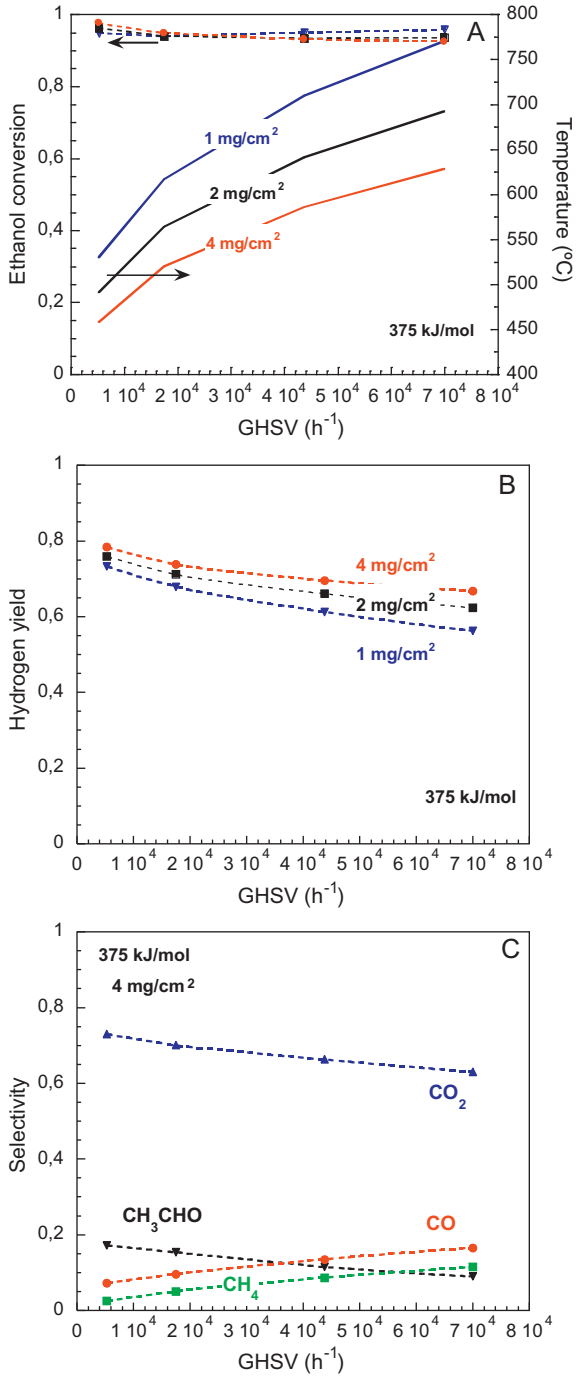

Fig. 3. (A) Ethanol conversion and mean reforming temperatures (solid lines). (B) Hydrogen yields. (C) Selectivities to CO_2, CO, CH_4 and acetaldehyde. Simulations were performed for microchannels with 0.70 mm of side, heating supply of 375 kJ/mol and catalyst loadings catalyst loadings (A and B) of 1 (blue), 2 (black) and 4 mg/cm^2 (red). (For interpretation of the references to color in this figure legend, the reader is referred to the web version of the article.)

4.2. Effect of the catalyst loading

Another series of CFD simulations was carried out over the model of the microreactor with channels of 0.70 mm of side at constant heating supply of 375 kJ/mol and catalyst loadings of 1, 2 and 4 mg/cm^2. The evolution with the GHSV of the ethanol conversion and reforming temperature, hydrogen yield and selectivities to the carbon-containing products for these simulations are shown in Fig. 3A, B and C, respectively. The most noticeable effects of the increase of the catalyst loading are the increase of the hydrogen yield and the decrease of the reforming temperature at the microchannels outlet.

The increase of the reaction rate associated to a higher catalyst loading results in an increased consumption of energy as reaction heat, and then, a decrease of the temperature. At GHSV of 70,000 h^{-1}, the outlet temperature decreases from 768 to 628 °C when the catalyst loading is increased from 1 to 4 mg/cm^2. The increase of the hydrogen yield is due to a better selectivity rather

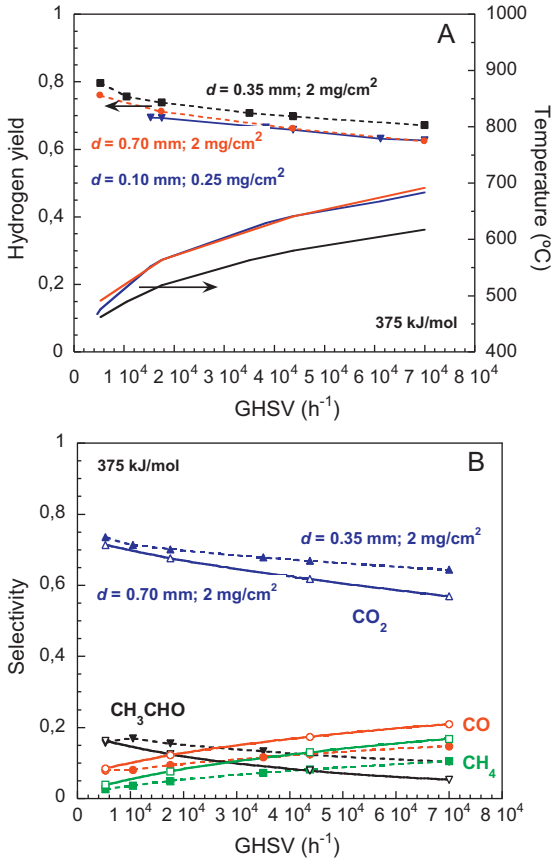

Fig. 4. (A) Hydrogen yield and mean reforming temperatures (solid lines) as a function of the GHSV for microchannels of 0.10 mm with 0.25 mg/cm^2 (blue), 0.35 mm and 2 mg/cm^2 (black) and 0.70 mm and 2 mg/cm^2 (red). (B) Selectivities to CO_2, CO, CH_4 and acetaldehyde for microchannels of 0.35 mm and 2 mg/cm^2 (dashed lines) and 0.70 mm and 2 mg/cm^2 (solid lines). (For interpretation of the references to color in this figure legend, the reader is referred to the web version of the article.)

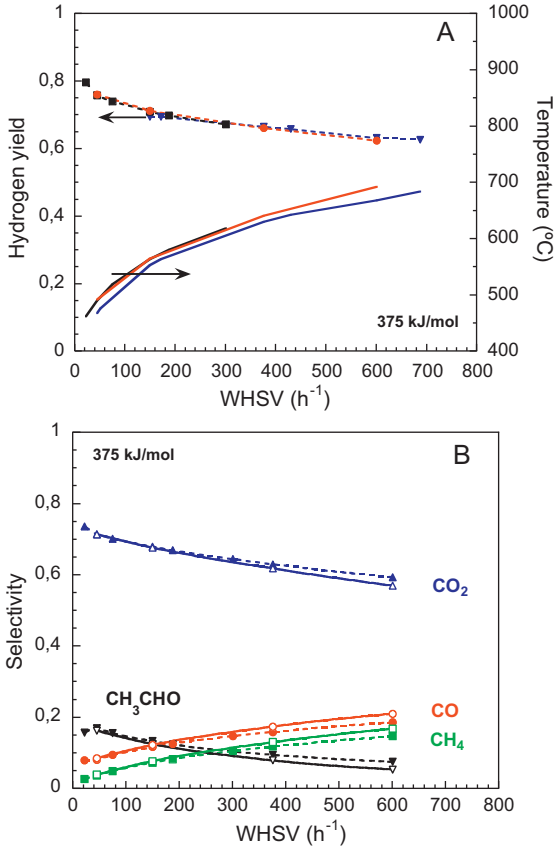

Fig. 5. (A) Hydrogen yield and mean reforming temperatures (solid lines) as a function of the WHSV for microchannels of 0.10 mm with 0.25 mg/cm^2 (blue), 0.35 mm with 2 mg/cm^2 (black) and 0.70 mm with 2 mg/cm^2 (red). (B) Selectivities to CO_2, CO, CH_4 and acetaldehyde for microchannels of 0.35 mm with 2 mg/cm^2 (dashed lines) and 0.70 mm with 2 mg/cm^2 (solid lines). (For interpretation of the references to color in this figure legend, the reader is referred to the web version of the article.)

than to a higher conversion. Actually the ethanol conversion remains almost unchanged as can be seen in Fig. 3A; in contrast, the selectivity to CO_2 increases significantly. For example, at GHSV of 70,000 h^{-1} the selectivity to CO_2 increases from 48% when using 1 mg/cm^2 of catalyst (Fig. 2C) to 63% with a loading of 4 mg/cm^2 (Fig. 3C). This means that the dehydrogenation of ethanol (Eq. (3)) and the steam reforming of acetaldehyde (Eq. (6)) compete more efficiently with the decomposition of ethanol (Eq. (4)) as the temperature becomes lower. This is due to the high apparent activation energy of this last reaction (see Table 1). This has another beneficial effect, namely, the decrease of the CO content in the reformate stream. Comparing Figs. 2C and 3C it can be seen that the selectivity to CO at GHSV of 70,000 h^{-1} decreases from 25 to 16% on increasing the catalyst loading from 1 to 4 mg/cm^2.

It can be concluded that increasing the catalyst loading is an efficient way to increase the hydrogen yield of the ESR in microreactors at high space velocities. In this regard, at the very high GHSV of 70,000 h^{-1} the hydrogen yield goes from about 57% when using 1 mg/cm^2 of catalyst to 67% with a loading of 4 mg/cm^2 (Fig. 3B), that is, from 3.4 to 4.0 mol of H_2 per mol of ethanol fed into the reactor. However, the possibility of increasing the catalyst loading is obviously limited by the microchannel size. Assuming a typical catalyst layer depth of 10 μm/mg/cm^2 of Co_3O_4–ZnO catalyst loading, the maximum value of 4 mg/cm^2 (40 μm of layer depth) used in this study can be considered reasonably low for a microchannel size of 0.70 mm (700 μm). In this work, internal diffusion effects in the catalyst layer have been neglected due to the small thickness of the layer which is estimated to be in the 10–40 μm range for catalyst loadings between 1 and 4 mg/cm^2.

4.3. Effect of the microchannel size

The influence of the characteristic size of the microchannels has been studied by comparing the results of CFD simulations performed with the models of the microreactors with channels of 0.70 and 0.35 mm of side with catalyst loading of 2 mg/cm^2 and the channel of 0.10 mm with only 0.25 mg/cm^2 due to its very low size. The evolution of the hydrogen yield and mean outlet reforming temperature with the GHSV are shown in Fig. 4A. It can be seen that, on a volumetric basis, the microreactor performance improves as the characteristic size decreases. In fact, the reforming temperatures are lower and the hydrogen yields higher for the channels with 0.35 mm of side compared with the results of the channels of 0.70 mm at the same catalyst loading. The performance of the channels of 0.10 mm is very similar to that of the ones of 0.70 mm but the catalyst content is 8 times lower. Therefore, the reduction of the characteristic dimension by a factor of 7 compensates this decrease of the catalyst loading. As concerns the selectivity, it can be seen in Fig. 4B that it is also more favourable for the channels of lower size because the selectivity to CO_2 increases and that to CO decreases for the channels with 0.35 mm of side compared with the ones of 0.70 mm. This improvement can be attributed to the lower reforming temperature, in a similar way as discussed in the preceding section for the effect of an increase of the catalyst loading.

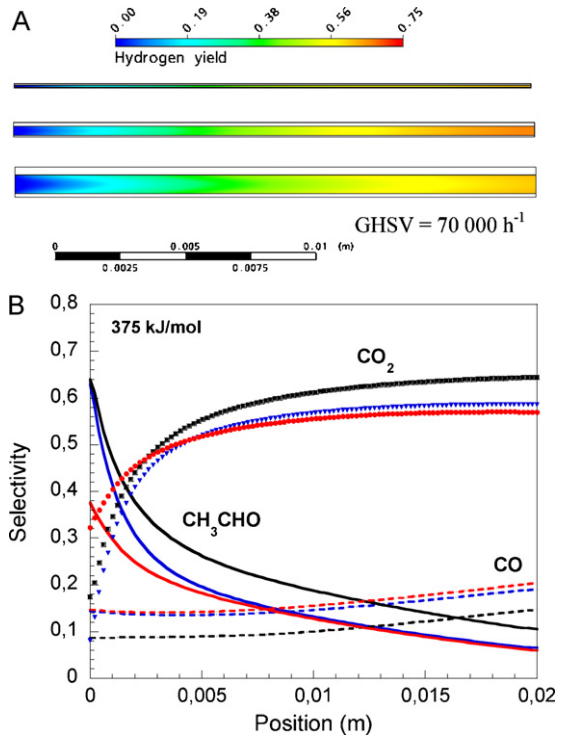

Fig. 6. (A) Hydrogen yields. (B) Selectivities to CO_2, acetaldehyde and CO for microchannels of 0.10 mm with 0.25 mg/cm^2 (blue), 0.35 mm with 2 mg/cm^2 (black) and 0.70 mm with 2 mg/cm^2 (red). (For interpretation of the references to color in this figure legend, the reader is referred to the web version of the article.)

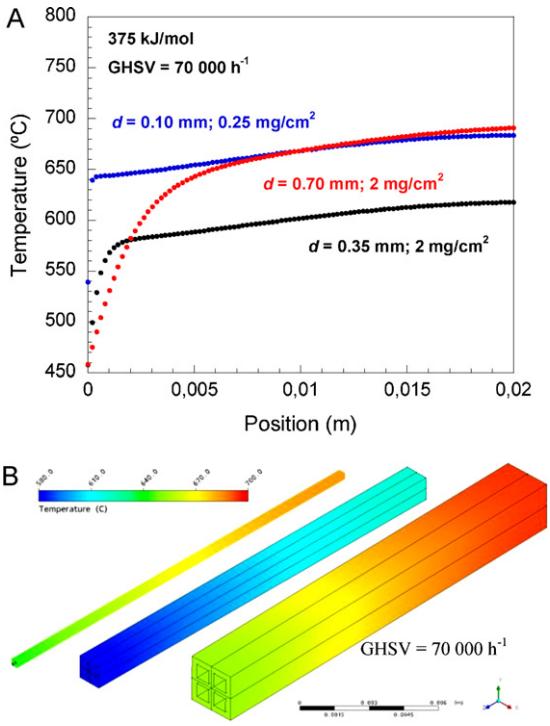

Fig. 7. (A) Fluid temperatures. (B) Solid block temperatures. Microchannels of 0.10 mm with 0.25 mg/cm^2 (blue), 0.35 mm with 2 mg/cm^2 (black) and 0.70 mm with 2 mg/cm^2 (red). (For interpretation of the references to color in this figure legend, the reader is referred to the web version of the article.)

To take into account the differences between the surface area-to-volume ratios associated to the three channel sizes considered as well as the catalyst loading effects, the performance of the microreactors has been compared also on a catalyst weight basis by means of the weight-hourly space velocity (WHSV). The results are shown in Fig. 5A and B. In this case, the differences between the hydrogen yields, reforming temperatures and selectivities almost disappear so it can be concluded that the performance of these microreactors for the ESR process is mainly dominated by the surface area-to-volume ratio which, in turn, depends on the microchannel size.

To illustrate the performance of the microreactors in this series of CFD simulations, Fig. 6A and B shows the evolution of the hydrogen yield and the selectivities to CO_2, acetaldehyde and CO along a central plane and a central line in the microchannels, respectively. It can be seen that the hydrogen yield increases progressively and slightly faster in the second half of the microchannel with 0.35 mm of side. As explained previously this results in an improved hydrogen yield at the channel outlet which is mainly due to the better selectivity (see Fig. 6B) obtained at lower reforming temperatures. The evolution of the selectivity to acetaldehyde clearly illustrates the role of this compound as intermediate of the ESR. Initially, acetaldehyde is the most abundant carbon-containing product as a result of the dehydrogenation of ethanol. This product is steam reformed along the microreactor (Eq. (6)) giving progressively higher hydrogen and CO_2 contents.

Regarding the reforming temperatures, their values along a central line inside the microchannels are shown in Fig. 7A. As can be seen, for the smallest channels (d of 0.10 and 0.35 mm), the temperature readily increases from 450 °C at the entry to a value close the outlet temperature so the flow is nearly isothermal. In the case of the channel with 0.70 mm of side the temperature changes along a broader portion of the channel although at half length its value is already close to the outlet temperature. Finally, the temperatures of the solid block are shown in Fig. 7B. In accordance with the fluid temperatures, it can be seen that in the solid with microchannels side of 0.35 mm the temperatures are the lowest; in this case, the maximum difference of temperature is about 30 °C. In the other blocks, the solid temperatures are between 40 °C (at the entry) and 80 °C (at the exit) higher. The maximum difference of temperature also increases up to about 50 °C.

5. Conclusions

A phenomenological kinetic model based on simple power-law rate equations and considering the following reactions: ethanol dehydrogenation to acetaldehyde, acetaldehyde steam reforming to H_2 and CO_2, ethanol decomposition to CO, CH_4 and H_2 and the water–gas shift, describes satisfactorily the ethanol steam reforming (ESR) over a Co_3O_4–ZnO catalyst. CFD simulations reveal that high reforming temperatures (above 625 °C) should be avoided because under these conditions the decomposition of ethanol competes effectively with the dehydrogenation of the alcohol to acetaldehyde, which is the key intermediate of the ESR process, and results in a reduced hydrogen yield and an increased content of CO in the reformate stream. In this work, it has been shown that microreactors can help to overcome these difficulties by increasing the surface area-to-volume ratio and the catalyst loading, which allow to reduce the operating temperature while increasing the selectivity and maintaining the level of ethanol conversion. Moreover, the use of microchannels with sufficiently low characteristic dimension (0.10–0.35 mm in this case) results in an almost isothermal flow and an effective control of the ESR temperature is attained, which preserve high hydrogen yields.

Acknowledgements

Financial support by the Spanish Ministry of Science and Innovation (MAT2006-12386-C05, ENE2009-14522-C04 and CTQ2009-

12520 grants) is gratefully acknowledged. I. Uriz gratefully acknowledges the fellowships granted by the Innovation Department of the Navarre Government and the Spanish Ministry of Science and Innovation (program FPI, BES-2010-030021).

References

[1] A. Haryanto, S. Fernando, N. Murali, S. Adhikari, Energy Fuels 19 (2005) 2098.
[2] P.D. Vaidya, A.E. Rodrigues, Chem. Eng. J. 117 (2006) 39.
[3] M. Ni, D.Y.C. Leung, M.K.H. Leung, Int. J. Hydrogen Energy 32 (2007) 3238.
[4] J. Rass-Hansen, R. Johansson, M. Møller, C.H. Christensen, Int. J. Hydrogen Energy 33 (2008) 4547.
[5] R.C. Saxena, D.K. Adhikari, H.B. Goyal, Renew. Sustain. Energy Rev. 13 (2009) 167.
[6] H. Idriss, M. Scott, J. Llorca, S.C. Chan, W. Chiu, P.Y. Sheng, A. Yee, M.A. Blackford, S.J. Pas, A.J. Hill, F.M. Alamgir, R. Rettew, C. Petersburg, S.D. Senanayake, M.A. Barteau, ChemSusChem 1 (2008) 905.
[7] G. Rabenstein, V. Hacker, J. Power Sources 185 (2008) 1293.
[8] P. Pfeifer, K. Haas-Santo, O. Görke, Application and operation of microreactors for fuel conversion, in: V. Hessel, A. Renken, J.C. Schouten, J.-I. Yoshida (Eds.), Micro Process Engineering, Vol. 2: Devices, Reactions and Applications, Wiley-VCH Verlag, Weinheim, 2009, p. 405.
[9] A. Qi, B. Peppley, K. Karan, Fuel Process. Technol. 88 (2007) 3.
[10] G.D. Stefanidis, D.G. Vlachos, Chem. Eng. Sci. 64 (2009) 4856.
[11] M. Karakaya, A.K. Avci, Int. J. Hydrogen Energy 35 (2010) 2305.
[12] L. Kiwi-Minsker, A. Renken, Catal. Today 110 (2005) 2.
[13] D.R. Palo, R.A. Dagle, J.D. Holladay, Chem. Rev. 107 (2007) 3992.
[14] G. Kolb, Steam reforming, in: V. Hessel, A. Renken, J.C. Schouten, J.-I. Yoshida (Eds.), Micro Process Engineering, Vol. 2: Devices, Reactions and Applications, Wiley-VCH Verlag, Weinheim, 2009, p. 421.
[15] M. Benito, R. Padilla, J.L. Sanz, L. Daza, J. Power Sources 169 (2007) 123.
[16] B.J. Bowers, J.L. Zhao, M. Ruffo, R. Khan, D. Dattatraya, N. Dushman, J.-C. Beziat, F. Boudjemaa, Int. J. Hydrogen Energy 32 (2007) 1437.
[17] T. Aicher, J. Full, A. Schaadt, Int. J. Hydrogen Energy 34 (2009) 8006.
[18] Y. Men, G. Kolb, R. Zapf, V. Hessel, H. Löwe, Process Saf. Environ. Protect. 85 (2007) 413.
[19] O. Görke, P. Pfeifer, K. Schubert, Appl. Catal. A: Gen. 360 (2009) 232.
[20] W. Cai, F. Wang, A. van Veen, C. Descorme, Y. Schuurman, W. Shen, C. Mirodatos, Int. J. Hydrogen Energy 35 (2010) 1152.
[21] A. Casanovas, M. Saint-Gerons, F. Griffon, J. Llorca, Int. J. Hydrogen Energy 33 (2008) 1827.
[22] A. Casanovas, C. de Leitenburg, A. Trovarelli, J. Llorca, Catal. Today 138 (2008) 187.
[23] A. Casanovas, M. Domínguez, C. Ledesma, E. López, J. Llorca, Catal. Today 143 (2009) 32.
[24] J. Llorca, A. Casanovas, T. Trifonov, A. Rodríguez, R. Alcubilla, J. Catal. 255 (2008) 228.
[25] A. Perna, Int. J. Hydrogen Energy 32 (2007) 1811.
[26] J.A. Francesconi, M.C. Mussati, R.O. Mato, P.A. Aguirre, J. Power Sources 167 (2007) 151.
[27] V.M. García, E. López, M. Serra, J. Llorca, J. Riera, Int. J. Hydrogen Energy (2009), doi:10.1016/j.ijhydene.2009.09.064.
[28] J.A. Francesconi, M.C. Mussati, P.A. Aguirre, Int. J. Hydrogen Energy 35 (2010) 5940.
[29] E. López, A. Irigoyen, T. Trifonov, A. Rodríguez, J. Llorca, Int. J. Hydrogen Energy 35 (2010) 3472.
[30] J.A. Torres, J. Llorca, A. Casanovas, M. Domínguez, J. Salvado, D. Montané, J. Power Sources 169 (2007) 158.
[31] M. Domínguez, E. Taboada, E. Molins, J. Llorca, Catal. Today 138 (2008) 193.
[32] D.W. Marquardt, J. Soc. Ind. Appl. Math. 11 (1963) 431.
[33] T. Glatzel, C. Litterst, C. Cupelli, T. Lindermann, C. Moosmann, R. Niekrawietz, W. Streule, R. Zengerle, P. Koltay, Comput. Fluids 37 (2008) 218.
[34] G. Arzamendi, P.M. Diéguez, M. Montes, M.A. Centeno, J.A. Odriozola, L.M. Gandía, Catal. Today 143 (2009) 25.
[35] G. Arzamendi, P.M. Diéguez, M. Montes, J.A. Odriozola, E. Falabella Sousa-Aguiar, L.M. Gandía, Chem. Eng. J. 154 (2009) 168.
[36] G. Arzamendi, P.M. Diéguez, M. Montes, J.A. Odriozola, E. Falabella Sousa-Aguiar, L.M. Gandía, Chem. Eng. J. 160 (2010) 915.
[37] A.A. Rostami, A.S. Mujumdar, N. Saniei, Heat Mass Transf. 38 (2002) 359.
[38] M. Wang, X. Lan, Z. Li, Int. J. Heat Mass Transf. 51 (2008) 3630.
[39] F.P. Incropera, D.P. De Witt, Fundamentals of Heat and Mass Transfer, John Wiley & Sons, New York, 2002, p. 931.
[40] R. de Cássia Colman, L.A. Torres, A.F.F. de Lima, L.G. Appel, Int. J. Hydrogen Energy 34 (2009) 9832.